An Improved Shape Memory Alloy Actuator for Rotor Blade Tracking

KIRAN SINGH,* JAYANT SIROHI AND INDERJIT CHOPRA

Department of Aerospace Engineering, Alfred Gessow Rotorcraft Center, University of Maryland, College Park, MD 20740, USA

The design, analysis, and testing of an improved Shape Memory Alloy (SMA)-based tracking tab actuator is described in this paper. The goal of the actuator is to provide in-flight tracking capability for a helicopter rotor in order to minimize 1/rev vibrations due to rotor dissimilarities. Previous SMA-based actuator designs demonstrated the potential for in-flight rotor tracking but admitted drawbacks that led to inconsistent operation under air-loads. The current research builds upon the existing knowledge base and addresses the challenges encountered in previous designs. The objective is to achieve a deflection of $\pm 5^\circ$ with an accuracy of 0.1° under realistic aerodynamic loading conditions. The present actuation concept is based on the bidirectional motion of a pair of antagonistic SMA wires, with a passive friction brake to lock the tab position. A theoretical model of the actuator was developed based on Brinson's thermomechanical model. The model was used to predict the behavior of the actuator under external loading and applied as a design tool to identify optimal actuator parameters. The actuator was integrated into a NACA 0012 12 in. chord blade section and tested in an open-jet wind tunnel at speeds of up to 120 ft/s (0.107 M) and at angles of attack up to 15°. Closed-loop tracking was implemented using a PID controller with gains selected by Ziegler-Nichols tuning. The improved SMA actuator meets the project goals by achieving repeatable tab deflection of up to $\pm 5^\circ$ with an average accuracy of 0.05°. Position hold under power-off conditions and a duty cycle of 20 cycles/h were also demonstrated.

Key Words: shape memory alloy, rotor tracking, active tracking, on-blade actuators, frictional lock

INTRODUCTION

An untracked rotor blade system is a common source of the large 1/rev vibrations in helicopters. Small dissimilarities in structural or aerodynamic properties of the blades created during the manufacturing process, or occurring as a result of wear results in the rotor system going out of track. The conventional procedure for rotor tracking is a ground-based method requiring adjustment of pitch links and tracking tabs. The difference in tip path plane between the rotor blades is measured while the rotor is spinning. The rotor is then stopped and tracking tabs and/or pitch links are manually adjusted. This procedure is repeated on a trial and error basis until the rotor is tracked to a sufficient accuracy. This conventional rotor tracking procedure is both time-consuming and expensive.

The tracking tab adjustment procedure is of pertinence to this particular study. Recently a few researchers Liang et al. (1996); Giurgiutiu et al. (1997) Gin have examined methods to replace the current manual tracking procedure with an on-blade tracking mechanism capable of deflecting a tracking tab in-flight. It is anticipated that an on-blade tracking system would effectively replace manual tracking operations and thus reduce operation errors, maintenance time and associated costs. Actuators based on high-energy density smart materials are ideally suited to this application because of severe volumetric constraints and low allowable weight penalties associated with mechanisms mounted on a rotor blade.

Shape memory alloys (SMA) are a class of smart materials that are particularly relevant to this application. The comparably large output force and stroke capability offered by SMAs enables the design of simple actuation mechanisms. This is in contrast to complicated designs requiring gear reduction or motion amplification when employing conventional materials or other smart materials, such as piezoelectrics. Low actuation voltages, low costs, and reduced number of moving parts are additional advantages associated with SMAs. These materials are temperature-activated and hence operate at low frequencies (less than 1 Hz). However, because tracking operations need not be conducted at high frequencies, the low bandwidth demonstrated by SMAs is more than adequate for this application.

*Author to whom correspondence should be addressed.
E-mail: ksingh@glue.umd.edu

1045-389X/03/12 0767–20 $10.00/0 DOI: 10.1177/1045389X03039134

Tab actuation systems implementing SMAs, which have been built and/or tested in the past, have demonstrated the anticipated advantages of these materials. These actuation systems may be broadly classified under two types, based on their deflection mechanism:

1. **Torsional tubes/rods** – Actuators implementing torsional tubes/rods develop rotational strains and moments, that are directly transmitted to the tracking tab. Liang et al. (1996) conducted a preliminary study to assess the feasibility of on-blade SMA torsional tube tab actuators and recommended several features for tab actuation. These have been quantified, tabulated, and discussed in ''Actuator Design Goals''. Kennedy et al. (2000) experimentally fabricated and tested a bidirectionally operating actuator assembly employing a pair of antagonistically operating SMA torsional tubes. The design employed appropriate heating and cooling hardware to actuate the SMA material. Test results indicated the system had the capability to accomplish the actuation goals. This design was however never tested under aerodynamic or centrifugal loads. From these two studies a primary drawback of actuation using SMA torsion tubes also becomes evident. Due to their large thermal inertia, torsional actuators require external heating and cooling systems for activation. The large volume occupied by these heating and cooling elements impedes the integration of the entire system into the confined space in a rotor blade section.
2. **Wire actuators** – The extensional strains of SMA wires are translated into a rotational motion of the tracking tab. Tab actuators employing SMA wires have been designed for operation in a hydrofoil by Rediniotis et al. (1999) and for rotor blade tracking by Giurgiutiu et al. (1997) and Epps and Chopra (2000). In contrast to torsion tubes, wires demonstrate a much smaller thermal inertia. This property permits faster thermal actuation of SMA wires. Additionally, internal resistive heating of the wires eliminates the need for bulky external heating mechanisms. Consequently, SMA wire-based actuators can be easily integrated into the blade section. The challenge associated with a design incorporating SMA wires, as observed from previous experience, is in designing an effective method of gripping the wires and therefore demonstrating consistent actuation behavior.

The actuator fabricated by Epps and Chopra (2000) was tested in the wind tunnel and displayed capability of actuation to $\pm 10^\circ$ in wind speeds up to 120 ft/s (0.107 M). This actuator comprised a bidirectional SMA wire design with a locking mechanism and a feedback position control system. The test results indicated the merits of this design, however, they also showed some drawbacks in the actuation system. These drawbacks were identified to be unequal tab deflection angles, lack of repeatable actuation, poor angular resolution due to discretization introduced by a geared locking system and inability of the locking mechanism to maintain angular position. Additionally, the control system employed a two-position control scheme. On detailed testing, this control scheme was found to be nonideal for a rotor tracking tab as a result of large tab position overshoots and unpredictable chatter under external loading. Overall the design of bidirectional actuation using SMA wires was established as effective for a rotor blade tab actuator. Therefore, the design of Epps and Chopra (2000) was selected as a baseline upon which to improve.

The objective of this study is to address and overcome the challenges encountered in the baseline tab actuation system, in order to achieve sustained and accurate tracking response. A more reliable method of clamping the SMA wires is demonstrated. The new actuator design incorporates a passive friction brake to maintain the tab position, which provides a fail-safe in case of power loss or actuator failure. The advantage of this brake is its infinite resolution and the ability to maintain tab position without the continuous supply of power. An analytical model of this actuator is developed for conducting a parametric analysis to size the actuator according to flight requirements. Finally, the actuation system is integrated into a blade section and tested in the wind tunnel to demonstrate the improved performance.

Actuator Design Goals

The parameters for designing the tracking tab actuator evolved from the expected angles and loads that were estimated to be experienced by the tracking tab, during operation on the rotor blade. Liang et al. (1996) and Kennedy et al. (2000) describe the tests conducted, to obtain a quantitative estimate of the structural and environmental conditions the actuator must operate in. The actuators were sized for a Boeing (McDonnell Douglas) MD900 helicopter (weight 6250 lbs). The goals that have evolved from the two studies are summarized in Table 1 and are described below.

Table 1. Tracking tab actuator goals.

	Goals
Actuator stroke	$\pm 5^\circ$
Resolution	$\pm 0.1^\circ$
Braking moment	4.0 in. lb
Actuator weight	< 1 lb
Actuator dimensions	10 in. $\times$ 8 in. $\times$ 1 in.
Duty cycle	20 cycles per h
Temperature range	-60 to 160°F

The actuator should conform to a weight of less than 1 lb, tab motion of $\pm 5^{\circ}$, resolution of $\pm 0.1^{\circ}$, output and braking moments (to overcome hinge moments due to aerodynamic and rotating frame loads) of 4.0 in. lbs, and a duty cycle of 20 cycles/h. The mechanism must be capable of meeting geometric design requirements imposed by space limitations of the 12 in. chord NACA 0012 blade profile. These spatial constraints were established to be a thickness dimension of 1.4 in. at the quarter chord section and 0.8 in. at the location of the hinge tube. The system should be capable of withstanding aerodynamic and rotating frame loads expected to be encountered near the 75% radius of the blade. Temperature, force (moment), and position (angle) sensors need to be located on the tab assembly, providing feedback to a position control mechanism. Additionally, sustained tab deflection under a power off-condition is required.

The overriding task set for this study was to eliminate the actuator inconsistencies observed in the baseline actuator designed by Epps and Chopra (2000). Thus the fundamental objective of this paper is to demonstrate the capability of the improved actuation system to achieve the identified tab actuator program objectives. However, since rotational frame testing is not a part of the present testing schedule, at this stage investigations of actuation under centrifugal forces have not been conducted.

ACTUATION SYSTEM COMPONENT DESIGN

The fundamental tab actuation principle is first addressed in this section and the individual components of the actuator are then examined. The primary elements that comprise this actuator are the wires, clamping mechanism for gripping the wires, a passive friction brake to maintain position and connection and prestrain mechanisms. Figure 1 shows some of the important features of the actuator assembly installed in the NACA 0012 blade profile.

Actuator Operating Principle

Figure 2 schematically illustrates the principle of operation of the actuation system tested. The wires are fixed rigidly at one end and are connected to a rotating hinge tube at the other, with upper and lower wires preloaded by an equal amount. The upper and lower wires are thermally and electrically insulated from one another and are resistively heated and air-cooled. Heating the upper set of wires results in a reduction in their length while the lower set of wires, maintained at room temperature, extend by an equal amount. This action results in a rotation of the hinge tube and deflection of the attached tab. The reciprocating motion of the wires may then be transmitted in this manner to the required deflection of the tab. The relationship is given by,

$$\theta = \left(\frac{L_o \epsilon_r}{r_{\mathrm{ht}}}\right) \tag{1}$$

where L_o is the length of the wires, ϵ_r is the strain in the wires and r_{ht} is the radius of the hinge tube. A reversal in heating results in the opposite action and therefore a downward deflection of the tab.

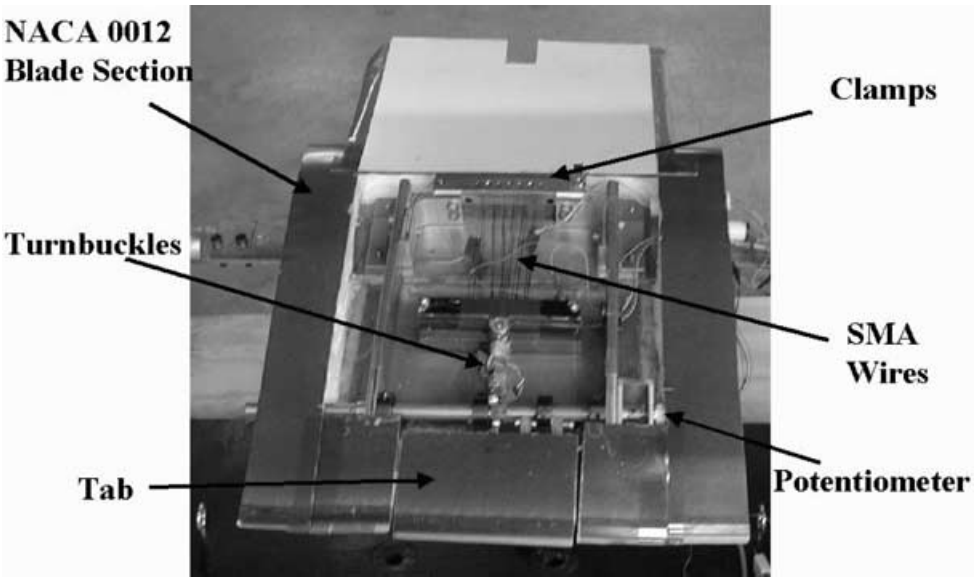

Figure 1. *Tab actuation system components.*

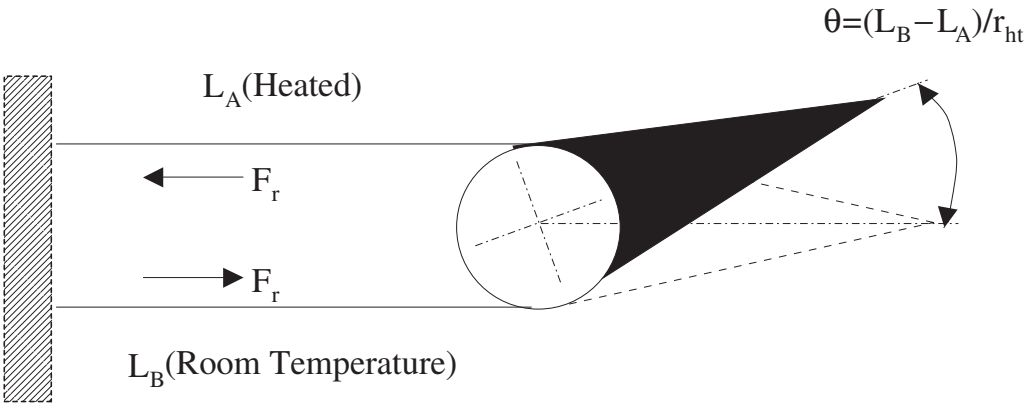

Figure 2. *Schematic of operation of dual shape memory alloy actuator.*

Actuator Assembly

CLAMPING MECHANISM

The clamping mechanism assembly was designed to restrain the SMA wires with the fore end fixed and the aft end free to move linearly in response to heating/cooling of the wires. The linear motion of the aft clamp is transmitted at the hinge tube to deflection of the tab. The assembly consisted of two pairs of stainless steel clamps where each set formed a framework for the upper and lower wires. One end of the clamp pair rigidly bolted on to the spar, the other end was free to slide along guide rails. Each clamp pair comprised two 1/8 in. thick stainless steel plates, with dowel pins embedded between them. The wire was wound around the dowel pins and back again in a manner such that each wire could be fixed at one end of the clamp. The purpose of this configuration was to implement segmentation of the SMA wire and hence effect force multiplication in the system. The advantage of gripping the single SMA wire at only one location was the reduction in multiple possible points of failure to one. Once the wire was prestrained, heat activation generated a reduction in wire length, which was transmitted to the movable clamps into linear sliding motion. The linear motion results in rotation of the hinge tube, which in turn deflects the tab. The SMA wires employed were of Nitinol (Ni-51%,Ti-49%) material (procured from Dynalloy, 2002). Figure 3(b) shows schematic details of this clamping mechanism.

It should be noted that for the present design, the emphasis was to reduce potential failure points due to multiple wires. The multiple wire design was partially responsible for the inconsistencies observed in the baseline actuator operation. For the current proof of concept stage, demonstration of consistent operation was weighed to be of higher importance than redundancy in design. Therefore the single SMA wire multi-segmented design was implemented.

CONNECTING ELEMENTS AND PRESTRAIN MECHANISM

The clamp output motion was transmitted to the deflecting tab through a pair of linkages. These comprised a pair of oppositely threaded rod-ends, connected to a threaded turnbuckle. The rod-ends were attached on to the movable clamp at one end and the rotating hinge tube at the other end. These turnbuckles had multiple roles to play in this design. Apart from transmitting the linear motion of the wires to deflection of the tab, rotating the turnbuckles also enabled a convenient method of prestraining the wires. Additionally, the turnbuckles were instrumented with full bridge strain gages to act as force sensors.

LOCKING MECHANISM

A locking device is necessary in order to maintain the tab position without further supply of power once the desired tracking position is acquired. The main specification for the lock was that it must allow for rotation in both directions as well as hold the hinge tube in position without slipping, under external loading. Several active friction brake designs employing piezostacks, electrostrictives, and SMAs were experimented with. Eventually a passive friction brake was selected as the final design. The passive brake consisted of a shaft collar, rigidly mounted on the rib and around the shaft. A torque wrench was used to tighten the collar to required friction settings. The passive brake was designed to prevent tab motion up to a preset braking moment while for actuation moments exceeding this braking moment, the hinge tube was capable of rotation.

BLADE SECTION ASSEMBLY

A NACA 0012 blade section of 12 in. span and 12 in. chord section was fabricated. The actuator was mounted into this blade section. The fabricated blade consisted of a foam core, trailing edge tab, and actuator assembly with spar and ribs to provide structural integrity. Teflon

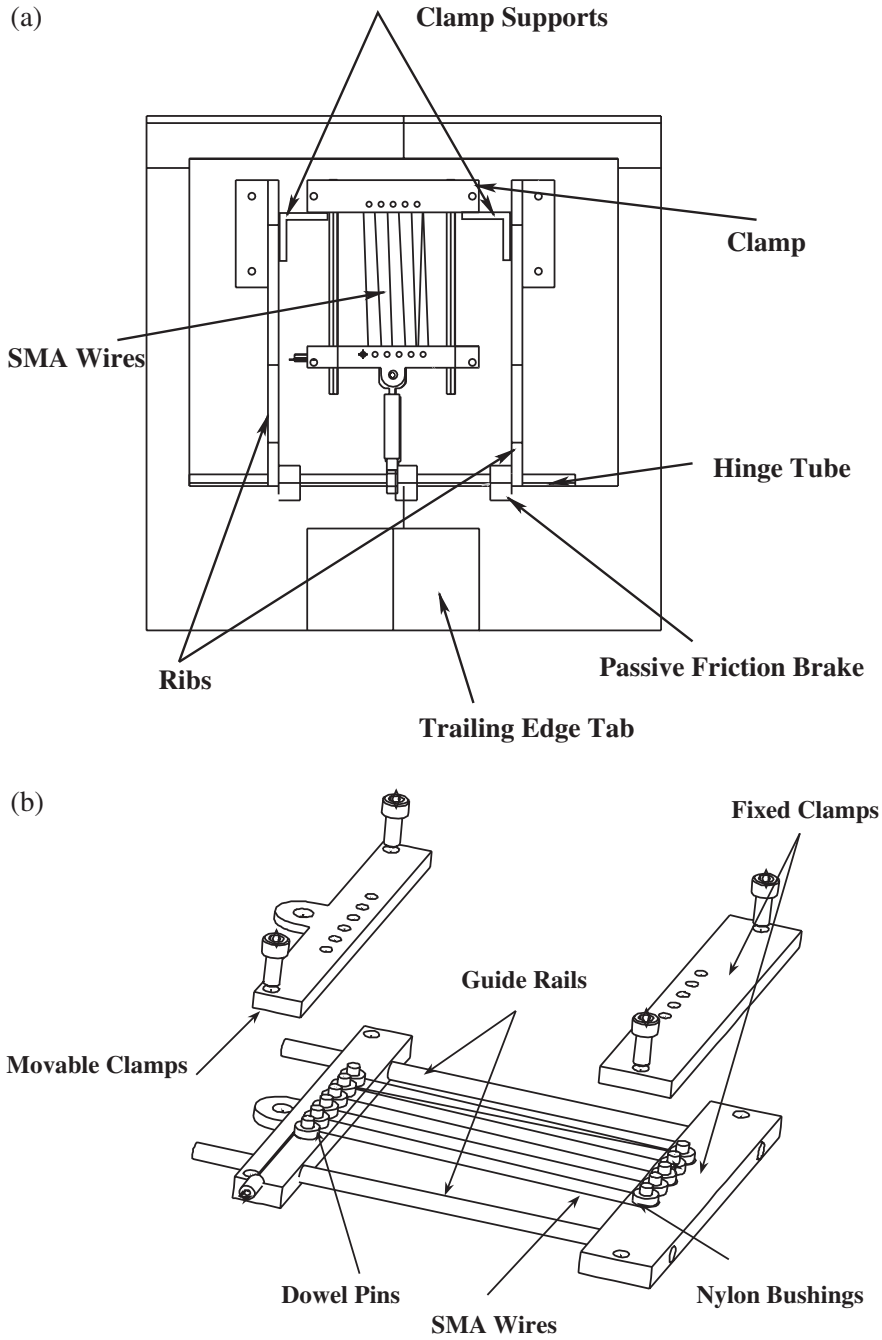

Figure 3. *SMA actuator components: (a) Top view of actual assembly; (b) SMA actuator clamping details.*

spring bushings were embedded at about 70% chordwise position and provided mounting points for the rotating hinge tube. Figure 3(a) schematically illustrates the actuator assembly installed in the blade section.

The tracking tab was embedded in the planform of the blade section and had a dimension of 4 in. span and 3.4 in. tab chord section. This is in contrast to existing tracking tab designs where the metal tab is typically 12–18 in. in span and projects out of the blade nominal planform. The motive for selection of the present configuration was primarily ease of fabrication. At present tab sizing considerations have not been dealt with. These issues are nonetheless important and are identified as an important future step towards clearly demonstrating feasibility of concept.

Position Feedback Controller

Closed-loop control was required to demonstrate the capability of the actuator to accurately deflect a tracking tab to the commanded input position. A control system was devised that could command an input tab position

(V_{SET}), measure the response in terms of tab deflection angle (V_{TAB}), and send corresponding actuation signals to the SMA actuator.

CONTROL SYSTEM DESIGN

A closed-loop PID controller was implemented using a LabView^{TM} Virtual Instrument, that performed functions of both data acquisition and control. The inputs to the controller were the measured tab position and the desired tab position, or setpoint. The error signal, V_{err} was calculated as the difference between the measured tab position and the setpoint. In the actuated state, the output of the controller was a voltage, $u(t)$, as defined by the classical PID control law in Ogata (1997),

$$U_{PID} = K_P V_{err}(t) + K_D \dot{V}_{err}(t) + K_I \int V_{err}(t)dt. \quad (2)$$

where K_P, K_I, and K_D are the proportional, integral and derivative gains respectively. These gains were determined for the present system by the Ziegler-Nichols method (Ogata, 1997) and are tabulated in Table 2. A small deadband Δ_{dead} was introduced in the controller, such that

$$\begin{aligned} u(t) &= 0 \quad \text{if} \quad |V_{err}| \le \Delta_{dead} \\ u(t) &= U_{PID} \quad \text{if} \quad |V_{err}| > \Delta_{dead} \end{aligned} \quad (3)$$

The deadband ensured that the output control voltage was zero when the tab position reached the desired position within the acceptable error margin. The output voltage served as an input to a power MOSFET driver that was connected to both sets of SMA wires. The sign of the output voltage determined which set of wires were to be actuated. It should be noted that for simplicity, the control voltage $u(t)$ was the gate-source voltage, V_{GS} of the output MOSFETS to which the SMA wires were connected.

DEVELOPMENT OF THE ANALYTICAL MODEL

The theoretical model discussed in this section implements the thermomechanical response of the SMA wires under applied stress and temperature within the actuator operating parameters. The model is developed in order to predict the behavior of this actuator when the wires are heat activated while operating within the constraints of the physical system.

Table 2. PID control gains.

Proportional gain, K_P	1.28
Derivative gain, K_D	8.0
Integral gain, K_I	0.051

The equations modeling this behavior and the parametric studies conducted applying the model, are discussed. The constraints imposed on the system are depicted in Figure 4 and the influence of the passive friction brake is clearly demonstrated in the stress–strain plots depicted in Figure 5.

Actuator Model Equations

The material behavior is fundamental to the actuation mechanism and is modeled in order to predict the output force and displacement of the tab actuator. For the sake of brevity in this discussion, the upper, heated wires are referred to as wire A and the lower wires, kept at room temperature, are referred to as wire B. For this analysis, the equations of motion are coupled with the transformation kinetic equations based on Brinson's (Brinson, 1993) thermomechanical model of a one-dimensional SMA specimen. This phenomenological model is developed to simulate the behavior of SMAs under the combined influence of temperature (T), stress (σ) and strain (ϵ) and the respective initial states. The constitutive law is developed here for a one-dimensional specimen, which relates the material parameters to the martensite volume fraction ξ. The constitutive equation for an SMA wire is given by the following equation,

$$\sigma - \sigma_o = E(\xi)\epsilon - E(\xi_o)\epsilon_o + \Omega(\xi)\xi_s - \Omega(\xi_o)\xi_{so} \quad (4)$$

where by definition,

$$\Omega(\xi) = -\epsilon_L E(\xi) \quad (5)$$

The stress and strain compatibility conditions define the states of the system during actuation. For wire A and wire B these are given as,

$$x^A = -x^B; \quad F^A = F^B + F_F \quad (6)$$

The basic steps of actuation are explained below:

1. **Prestrain Step:** The prestraining method specifies the initial conditions of the SMA wires, prior to heating. This is illustrated on the stress–strain curve in Figure 5 as the dotted line (XP'). Both wires are prestrained equally to ensure symmetric operation. The initial conditions are defined as,

$$\epsilon_o^A = \epsilon_o^B = \epsilon_o \quad (7)$$

$$\sigma_o^A = \sigma_o^B = \sigma(\epsilon_o) \quad (8)$$

The following approximation is made in the model, in order to define the initial volume fraction of the material,

$$\xi_{SO} = \frac{\epsilon_o}{\epsilon_L} \quad (9)$$

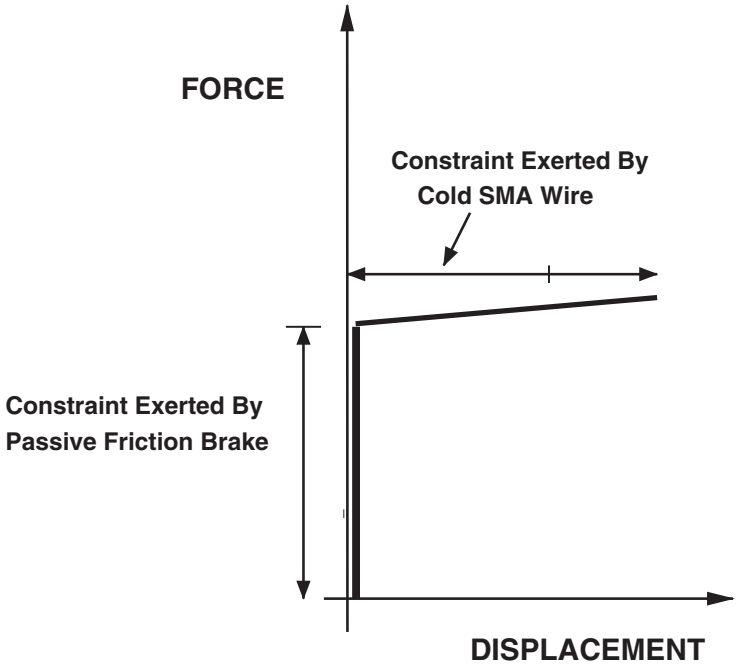

Figure 4. *Constraints imposed on the active SMA wire upon heat activation.*

2. **Heating – Zero Tab Deflection Condition:** Wire A is heated ($M \rightarrow A$ transformation) and undergoes constrained recovery until the stress in A overcomes the stress corresponding to the frictional moment (path $P'P$ in Figure 5) and is mathematically given by Equation (4). In this state there is no change in stress or strain of wire B (point P') as the following stress condition holds,

$$\sigma^A - \sigma^B < \sigma_F \tag{10}$$

3. **Heating – Tab Deflection Condition:** As the temperature of the wire rises, the transformation to austenite introduces stress in wire A to a level sufficient to overcome the frictional force. The actuating wire A is now able to exert a stress on wire B where this condition is represented by,

$$\sigma^A = \sigma_{\mathrm{F}} + \sigma^B \tag{11}$$

The strain developed in each wire is symmetric with respect to the prestrain ϵ_o,

$$\begin{aligned} \epsilon^B &= \epsilon_o^B + \epsilon_r \\ \epsilon^A &= \epsilon_o^A - \epsilon_r \end{aligned} \tag{12}$$

The fundamental difference in the state of the two wires is represented in the differing volume fractions of the two wires,

$$\begin{aligned} \xi^B &= 1 \\ \xi^A &= \xi(T^A, \sigma^A, \epsilon^A) \rightarrow 0 \end{aligned} \tag{13}$$

The transformation kinetic equations as developed by Brinson's model, define the martensite fraction for the two wires. Newton–Raphson's iterative technique is applied to solve Equations (4)–(12) simultaneously with the transformation equations with the objective of determining the thermomechanical parameters for the system.

The moment at the shaft in the counter clockwise direction is,

$$\tau = \left(\sigma^A - \sigma^B\right) \frac{\pi d_o^2}{4} N_{\mathrm{wire}} r_{\mathrm{ht}} \tag{14}$$

The strain recovery condition results in a deflection of the tab, the magnitude of which is represented by Equation (1).

Design iterations of this model were conducted to obtain the optimal actuator parameters and to assess the influence of external (aerodynamic) loads on the tab deflection angles and braking moment. The parametric studies and model correlation with experimental results are discussed in the next section.

PARAMETRIC STUDIES

The role of these parametric studies is to define parameters that allow design of an actuator that may be capable of achieving target output goals under the operating constraints. The method involves identifying

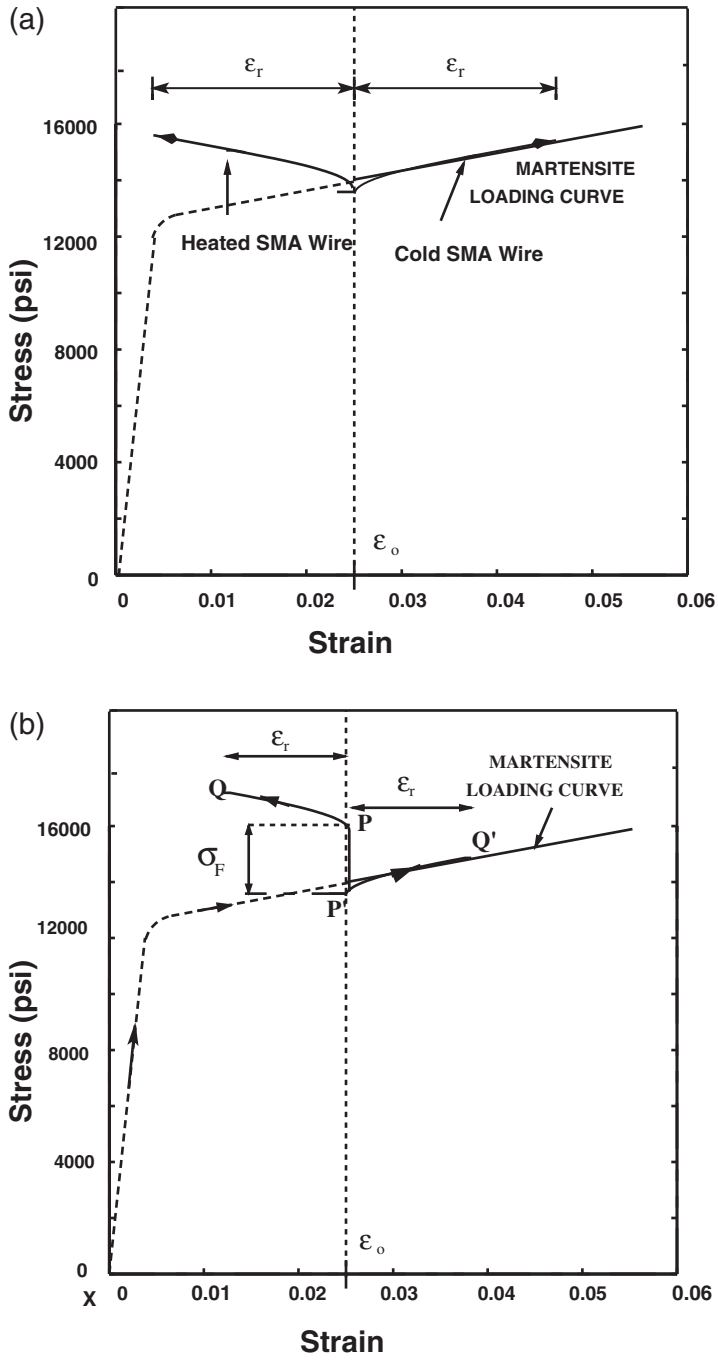

Figure 5. *Stress–strain plot with SMA wire boundary condition: (a) Zero friction case; (b) nonzero friction case.*

important actuator parameters and iterating the values of these parameters using the analytical model in order to achieve the desired performance. The ultimate objective is to implement the suitably-sized actuator assembly into a NACA 0012 12 in. chord blade section and to ensure deflection capabilities of $\pm 5^\circ$ under loading conditions of 120 ft/s (0.107 M) wind speeds at a maximum angle of attack of 15°. This extreme loading condition corresponds to a hinge moment of 0.85 in. lb.

Actuator Design Perspective

The actuator parameters identified are classified by their influence on either the angular rotation or actuation moment. To analyze the influence of actuator parameters on actuator output (tab deflection angle and braking moment), Equations (1) and (14) are used. The length of wire (L_o), radius of hinge tube (r_{ht}) and maximum recoverable strain (ϵ_r) directly influence the angular deflection (θ). The maximum recoverable strain

(ϵ_r) is in turn a function of the prestrain imparted to the wires (ϵ_o). The parameters affecting the actuation moment (τ) are the diameter of the wires, (d_o), radius of hinge tube, (r_{ht}) and the number of wire segments (N_{wire}).

Parameters Selection

The basis for selection of various design parameters is discussed below:

OUTPUT GOALS

The tab actuator goals as identified by Liange et al. (1996) and Kennedy et al. (2000) for an MD900 (6250 lb weight class) helicopter, impose definitive tab deflection and actuation moment requirements. The design requirements for this actuator are defined to be braking moments of 4 in. lbs and tab deflections of $\pm 5^\circ$. These requirements define the expected hinge moments the actuator would need to overcome as well as the capability to actuate at the 75% radial location of a rotating blade.

AERODYNAMIC REQUIREMENTS

In the present study, the actuator is tested solely under aerodynamic loading in an open-jet wind tunnel. To estimate the trailing-edge tab hinge moments due to aerodynamic loading, a model assuming quasi-static deflections is adopted (Walz and Chopra, 1994; Singh, 2002). From the predicted hinge moments, the actuator stroke/force capability is calculated for the design configuration employed. The expression for the total hinge moment for a simple plain blade section is given by:

$$H = \frac{1}{2}\rho V^2 c_f^2 l_f \left[C_{l_\alpha} \frac{dC_h}{dC_l}\left(\alpha_o + \frac{\Delta\alpha}{\Delta\delta}\delta\right) + \frac{dC_h}{d\delta}\delta \right] \quad (15)$$

where dC_h/dC_1 and $dC_h/d\delta$ are obtained as a function of (c_f/c), the details for these are obtained from Abott and von Doenhoff (1959). Note that c_f is the flap chord, l_f is the flap length, and δ is the flap deflection angle. Equation (15) represents a steady hinge moment necessary to maintain a given tab deflection angle. The quasi-steady analysis adopted, is considered sufficient for this application as tab deflections occur at a slow rate of less than 1 Hz From this equation, a hinge moment of 0.85 in. lbs is calculated for maximum loading conditions of V=120 ft/s (maximum tunnel speed, 0.107 M) at angles of attack of 15°. These imposed the requirement that tab deflection angles of $\pm 5^\circ$ are to be attained with an imposed braking moment of 0.85 in. lbs.

MATERIAL CONSTRAINTS

The deflection angle is a function of the recoverable strain, which in turn is a function of the prestrain imparted. The material thus imposes a restriction on the maximum prestrain that can be applied. For the SMA wire selected, this prestrain is set at 2.5% and a wire diameter of 15 mil. The wire diameter is selected based on the availability of material data (characterized in-house by Prahlad and Chopra, 2001).

GEOMETRIC CONSTRAINTS

The required capability of the actuator for deflecting the tab, while completely embedded in the blade section, imposes a finite constraint on actuator dimensions. A NACA 0012 blade profile with a chord and span of 12 in. is employed and the hinge tube is situated at the 72% chord location with the spar embedded into the blade, from 10 to 30% chordwise position. A major constraint on the actuator size is imposed along the thickness direction, which ranges from 1.2 to 0.85 in., depending upon the chordwise location. Hinge tube radius (r_{ht}) is hence governed by the space available at the 72% chord location. To satisfy this condition, the parameter r_{ht} is fixed at 0.35 in. The wire length (L_o), although constrained by the available chordwise dimensions, does allow a certain margin of variation, between 3.4 and 3.7 in. The second parameter available for variation is the number of wire segments, (N_{wire}). This forms an important parameter which may vary over a fairly large range (2–20 wires for the present configuration). Thus, this forms a chief control parameter and is iterated to obtain the actuation moment and angular deflection required for these tests.

Results of Parametric Studies

The key results obtained on varying frictional moment (τ_{F}), wire length (L_o) and the number of wires (N_{wire}) are examined here. The influence of varying these parameters is then quantified in terms of wind speed.

1. **Brake friction,** τ_{F}: has a direct impact on basic actuator parameters of angular deflection and external output moment. It is observed that actuation moment increases as the frictional moment to be overcome increases, while the range of available angular deflection decreases. This trend is shown in Figure 6, where the effect of increasing external loading moment is plotted.
2. **Number of wires,** N_{wire}: Figure 7 shows the influence of increasing the number of wires on the actuator output characteristics. The other control parameter wire length (L_o) is kept constant during iterations for this specific case. From Equations (1) and (14), it is evident that an

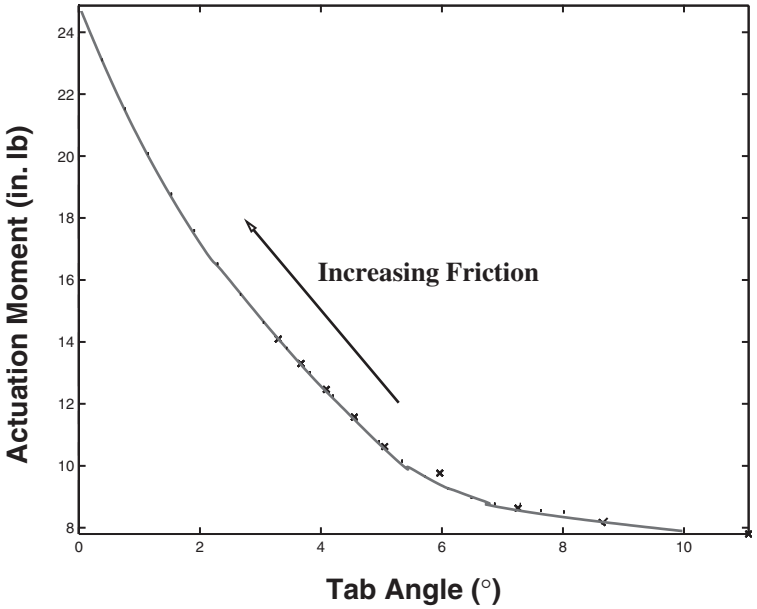

Figure 6. *Actuator output for increasing brake friction (zero wind speed, number of wires = 12).*

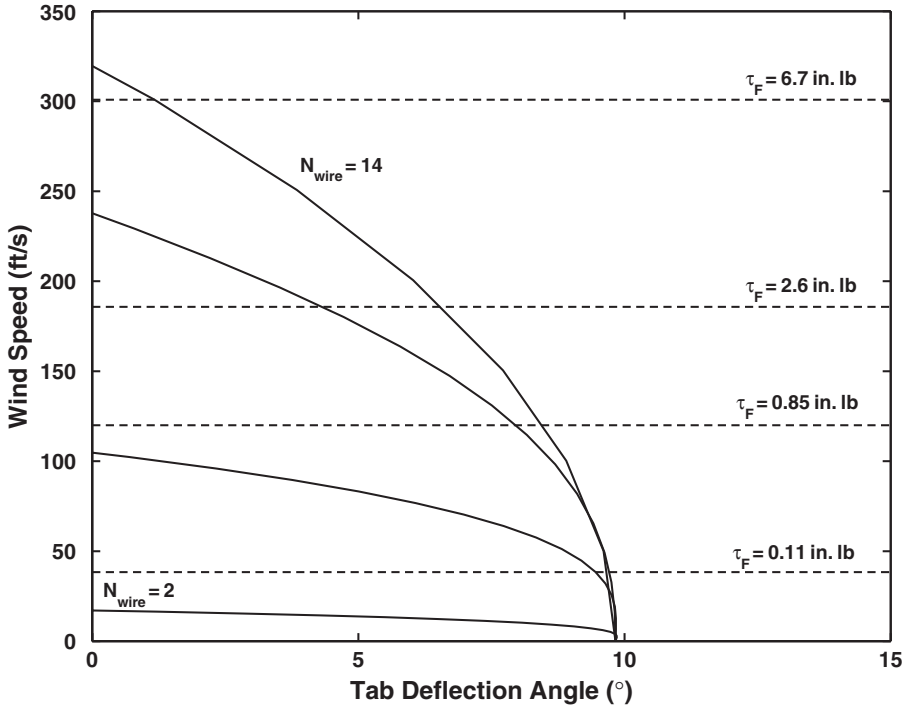

Figure 7. *Influence of number of wires, N_{wire}, on actuator characteristics (wire length = 3.6 in.).*

increase in N_{wire} increases the maximum actuation moment while it has no effect on maximum angular deflection. The wind speeds the actuator could operate at are shown in Figure 7. It should be noted that actuator operation constitutes effecting tab deflection at the operating wind speed as well as maintaining that deflection. Therefore the actuator must deflect the tab under both the air loads and the brake loads that correspond to the operating wind speed. The horizontal lines in Figure 7 define the maximum wind speeds for effective operation of the passive brake, as tuned to corresponding brake moments. From this figure it can be concluded that tab actuation under higher wind speeds is possible by increasing the control parameter (N_{wire}).

3. **Length of wire,** L_o: In Figure 8, the effect of varying the wire length L_o is examined, while maintaining the

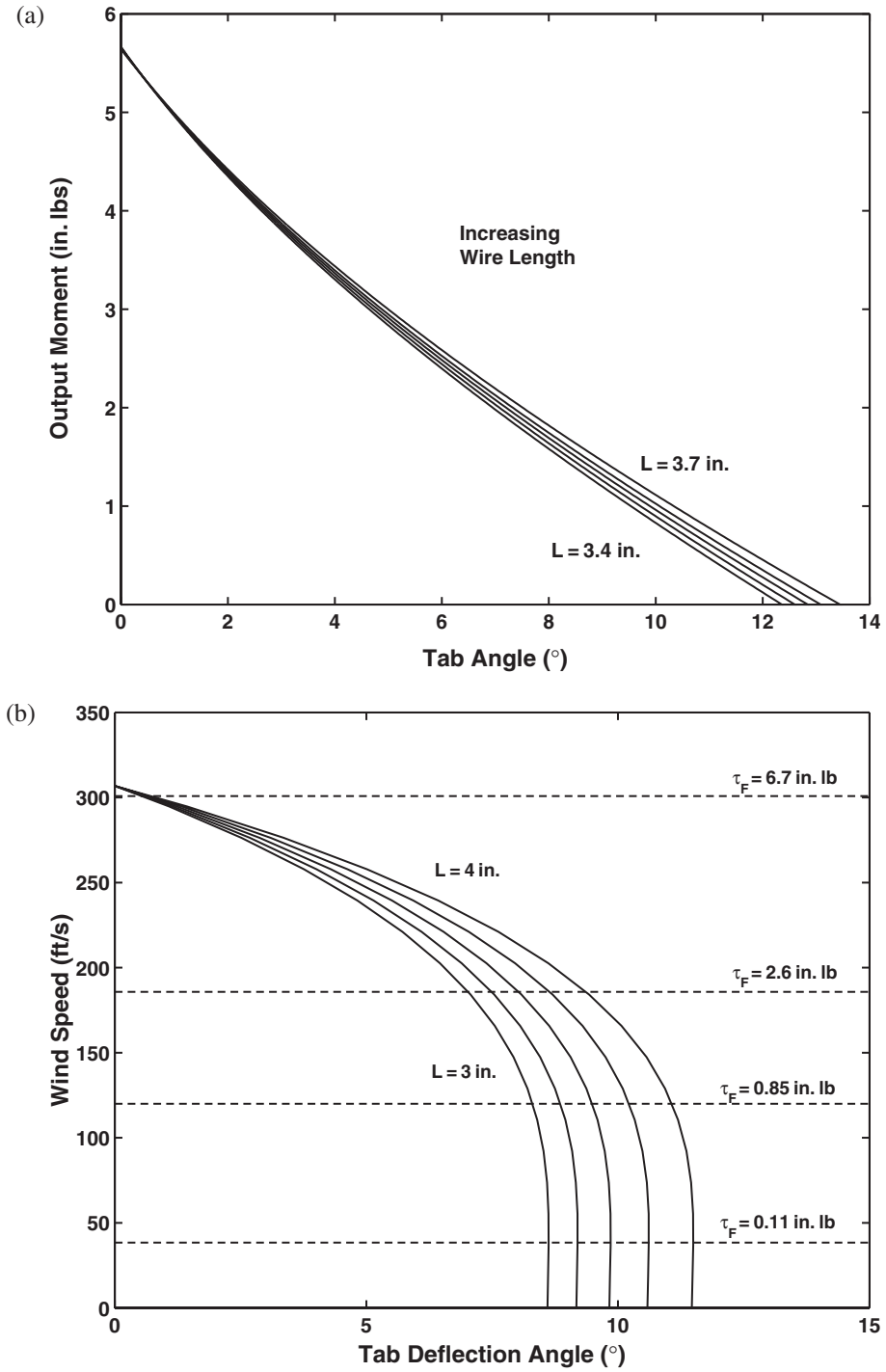

Figure 8. *Influence of wire length, L_o, on actuator characteristics (Number of wires = 12): (a) Effect on actuator moment; (b) effect on maximum wind speed.*

number of wires (N_{wire}) at a constant. The increase in L_o increases maximum angular deflection, while it does not influence the maximum actuation moment. In Figure 8(b) this trend is quantified in terms of actuation wind speeds the actuator can operate in. It is important to note that for this formulation as well, tab deflection was calculated for corresponding air loads and brake loads.

It is worth noting that based on the parametric plots and the fact that there is a limited scope for varying the parameter L_o, the number of wires N_{wire} becomes a key parameter in influencing maximum achievable actuator output moment and thus maximum operating wind speed. The above set of parameters were iterated until acceptable values were obtained. The final set of parameters selected are tabulated in Table 3. It is worth noting

Table 3. Design parameters for constructing actuator.

Length of SMA wire	L_o	3.6 in.
Diameter of wire	d_o	0.015 in.
Radius of hinge tube	r_{ht}	0.35 in.
Braking moment	τ_F	0.85 in lb.
Range of tab deflection	θ_{max}	$\pm 5^\circ$
Number of wires	N_{wire}	12
Input power	P	3–4.5 W

that an increment in the number of wires is possible by simply scaling up in the spanwise direction without incrementation of actuator chordwise or thickness dimensions. Thus for the same blade, incrementing actuator dimensions only along the spanwise direction should yield full scale control authority. This presents a justification for the present approach of testing deflection capability of the actuator sized for operating at the maximum wind speeds generated in the open-jet tunnel.

EXPERIMENTAL TEST RESULTS

Open and closed-loop tests were carried out on the actuator to ascertain the ability to achieve the target goal of $\pm 5^\circ$ tab deflections with an accuracy of 0.1°, under aerodynamic loading. The first set of experiments involved validating the theoretical model by comparing predicted results with test data obtained under open-loop control conditions. Closed-loop tracking tests, implementing a PID control scheme were then conducted for target design conditions on the bench-top. Aerodynamic loads were simulated on the bench-top by hanging deadweights from the tab. The actuator was then integrated in a 12 in. chord blade section with a tracking tab and tested in an open-jet wind tunnel. The tests were carried out at four different wind speeds and two sets of angles of attack, to test actuator performance under aerodynamic loading conditions.

Open loop Tests

The open-loop tests were conducted in order to evaluate the accuracy of the analytical model by comparing with test results. The basic test equipment employed were type K thermocouples to measure the temperature of the two sets of wires. The tab deflection angle was measured using a three-quarter turn 10 KΩ potentiometer and the force was measured using two instrumented links. The signals from the sensors were measured using a data acquisition DSP, SIGLAB system interfaced with MATLAB and operated on a Pentium-III 900 MHz processor. In these tests, wire temperature was controlled using a Hewlett Packard 6642-A DC power supply rated at 10 A, 20 V. The current was set at 3 A with the voltage rate set at 0.017 V/s, in order to maintain a heating rate of 0.5°F/s. This corresponded to a strain rate of 0.0004/s during the heat activation cycle, while the opposing wire was maintained at room temperature. Experimental results were recorded over a period of 600 s. The power requirements of the actuator were calculated based on the maximum voltage and current requirements over the complete test range and were found to vary over a range of 3–4.5 W.

Figure 9 shows a comparison of predicted results with test data for zero braking moment. Figure 9(a) shows the tab deflection variation with temperature while Figure 9(b) depicts the actuation moment variation with tab angle. It is observed that the model captures the actuator behavior fairly well. The influence of the passive friction moment on the actuator was evaluated next and comparisons between experimental and theoretical results were made by increasing the friction moments imposed on the actuator. The screw setting on the friction brake was previously calibrated with a torque wrench. For each set of tests the friction imparted by the brake was incremented by adjusting the screw according to calibration. The maximum deflections and moments achieved were then compared with the analytical results in Figure 10. Possible explanations for the discrepancies between the model and experimental data, could be the assumptions that were made in developing the model. The assumption of the brake as a quasi-static friction may not be adequate. Static and dynamic friction can be different and careful testing is required to develop precise models. This might account for the over-prediction of strains at higher frictional moments. On average, the basic trends with varying friction are captured. These results provide an estimate of tab deflection angles achievable by the actuator, under corresponding braking moments.

Closed-loop Tests

The main objective of the closed-loop tests was to demonstrate the capability of the actuator to accurately deflect the tracking tab in response to commanded inputs. The position control system discussed in ''Position Feedback Controller'' was implemented to test closed-loop performance on both the bench-top and under aerodynamic loading conditions. The tests were conducted to examine this capability under aerodynamic loading corresponding to a wind speed of 120 ft/s at angles of attack up to 15°.

BENCH-TOP TESTS

The control system, discussed in ''Control System Design'' was employed and tab angular measurements

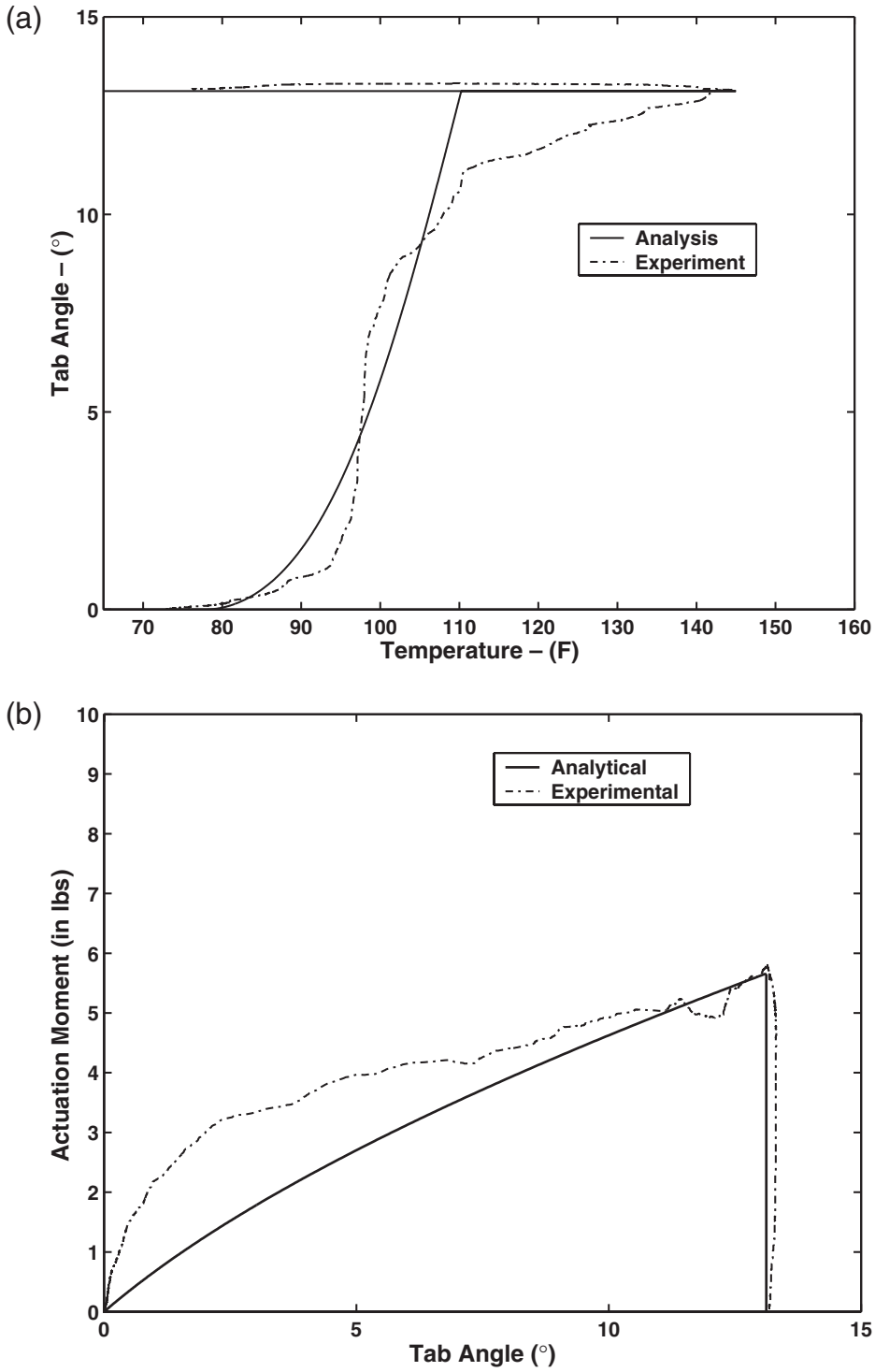

Figure 9. *Comparison of analytical model with test data.*

were carried out using a Hall effect sensor. Temperature of the wires was measured using Type K thermocouples. A Windows-NT-based Pentium III, 450 MHz PC equipped with a National Instruments, PCI-6031E, 16 bit DAQ card was used with a virtual instrument application, programmed using LABVIEW^{TM} 5.1. Five input channels to the DAQ measured temperature and angular rotation of the tab, while the actuating signals to the wires were sent through two output channels. The sampling period of the DAQ system was selected to be 1.5 s which was determined to be adequate for these quasi-steady tests.

The bench-top tests were conducted under zero load and under simulated external loads. For the simulated

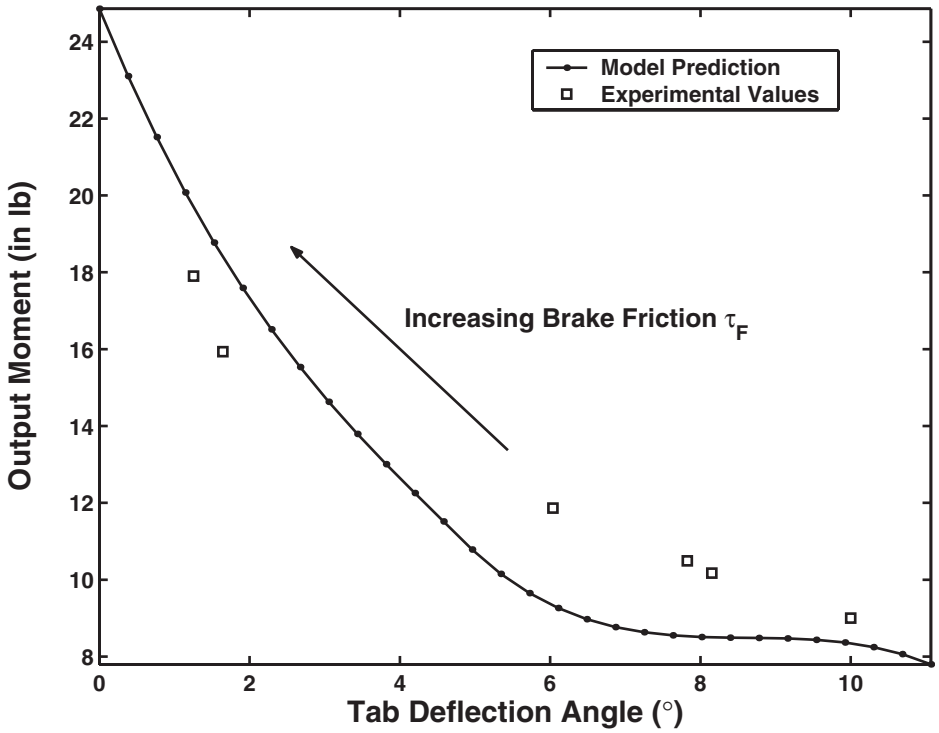

Figure 10. *Zero external load actuator curve – comparison of predicted value with experimental results obtained from open-loop test data (number of wires = 12).*

loading case, a dead weight was mounted at the tip of the tab, perpendicular to the blade chord. The maximum moment imparted was 0.85 in. lbs at the hinge tube. This corresponded to the maximum loads anticipated in the open-jet tunnel (for 120 ft/s, 15° angle of attack conditions).

The results of the zero and maximum simulated loading conditions are compared in Figure 11, for position accuracy and power-off capability. In Figure 11(a), the steady state error is compared for the two loading cases. Tab deflection is obtained within 0.07° of desired angle. For the same set of tests, the percentage change in steady state temperature from the ambient, is plotted in Figure 11(b). This figure demonstrates that the power to the actuators is turned off once the desired tab angle is reached, while the tab position is maintained by the brake. Therefore, it can be concluded that the actuator is functioning as designed. Figure 12 displays the response time of the tracking operation as the actuator responds to commanded inputs, under zero and maximum simulated loading conditions. The error bands in Figure 12(b) indicate the noise level of the tab angle sensing equipment. It may be observed that there is no overshoot of feedback response and it converges in less than 200 s for a no load condition and less than 500 s for a loaded condition. Even though this appears to be a very slow response, absence of overshoot is a significant advantage for rotor tracking.

It is observed from these plots that the system under closed-loop PID control, is capable of achieving the target steady state error and steady state temperature specifications (indicating power off condition). Moreover, simulated loading conditions did not suggest any significant degradation in performance in the operation of the actuator under either control action. This suggests the capability of the actuation system to maintain its position as well as to actuate the tracking tab under maximum wind loading conditions anticipated in the open-jet tunnel.

WIND TUNNEL TESTS

The tracking tab actuator was tested in an open test section wind tunnel. The wind tunnel has a rectangular test section of dimensions 22 in. × 22 in.. A maximum free-stream velocity of 120 ft/s could be achieved while the minimum idling speed was 30 ft/s. A pitot tube was used to measure the free-stream air speed. The data acquisition system used for these tests was identical to that used in the bench-top tests. Figure 13 shows the blade section mounted in the wind tunnel. The objective of these tests is to evaluate the performance of the actuator under aerodynamic loading. Closed-loop tracking tests were conducted for four different wind speeds, from 0 to 120 ft/s (0.107 M) and two varying blade angles of attack, 0° and 15°. To test the closed-loop tracking ability of the actuator, an input signal of +5° was initially commanded. After an interval of time, during which the actuator was allowed to settle to its steady state condition, an input of 0° was sent, followed by a −5°

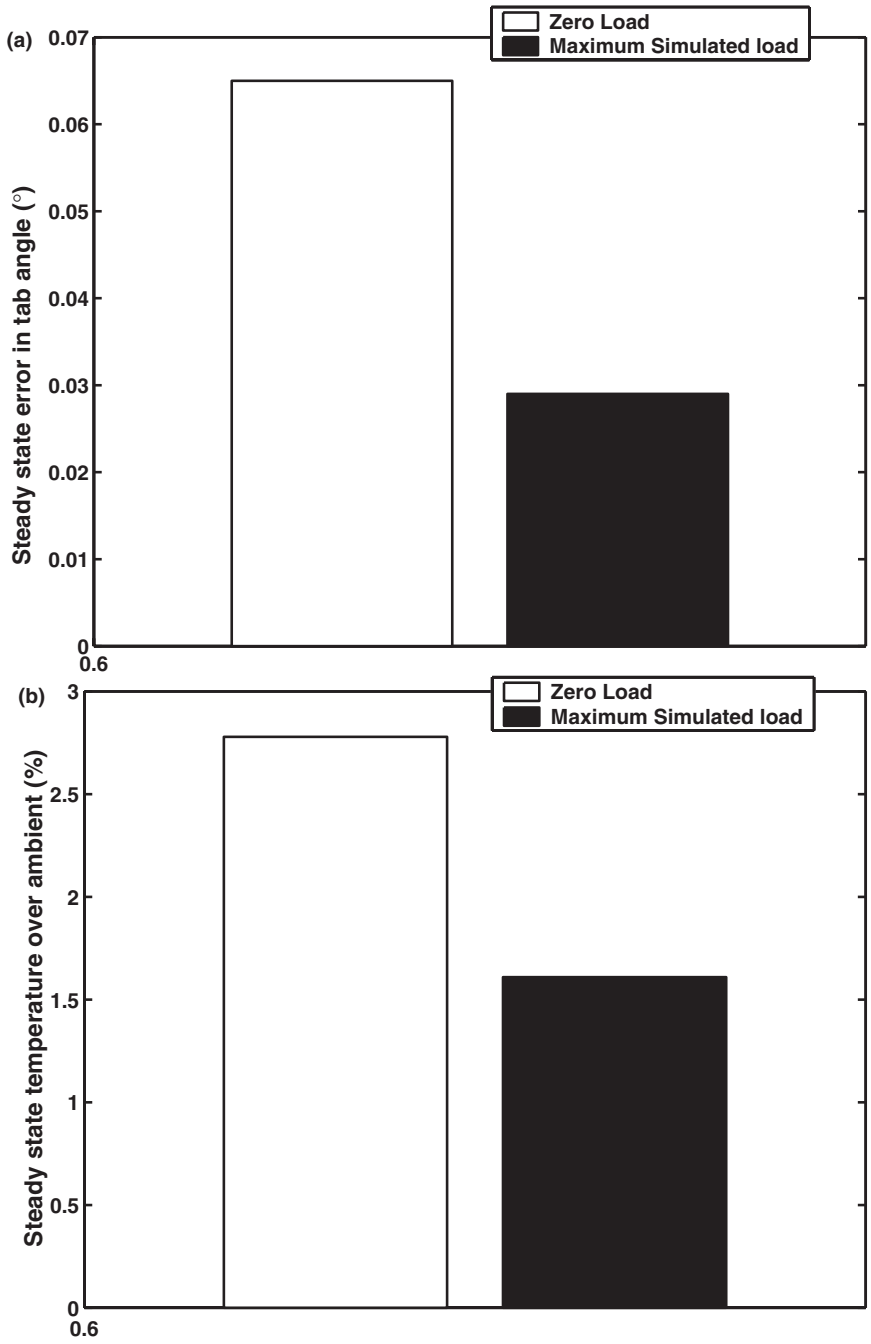

Figure 11. *Comparison of steady-state bench-top test results under zero and maximum simulated load conditions: (a) Steady state error; (b) steady state temperature (percentage increment over ambient conditions).*

input signal. This testing schedule was employed for all wind conditions under which the actuator was tested. Figure 14 plots steady-state results for all these test cases. In Figure 14(a) steady-state error in tab angle is shown. Superimposed on these plots are horizontal lines indicating the deadband. Steady state error was less than 0.05° for practically all wind speed/angle of attack cases and temperature difference (Figure 14(b)) results indicated that the tracking of tab to frictional brake is accomplished successfully and power-off condition was achieved. It should be noted that on an average, the PID controller achieved good results for all tested loading conditions with a constant set of control gains. However if better tracking performance is desired at specific loading conditions, the control gains may be changed as a function of the operating condition to yield optimum overall performance.

Figure 15 plots time histories of the tracking response for some representative wind conditions. The commanded signal is indicated by the dashed line in these plots, while the actuator response signal is the solid line. From these time traces it is evident that the system

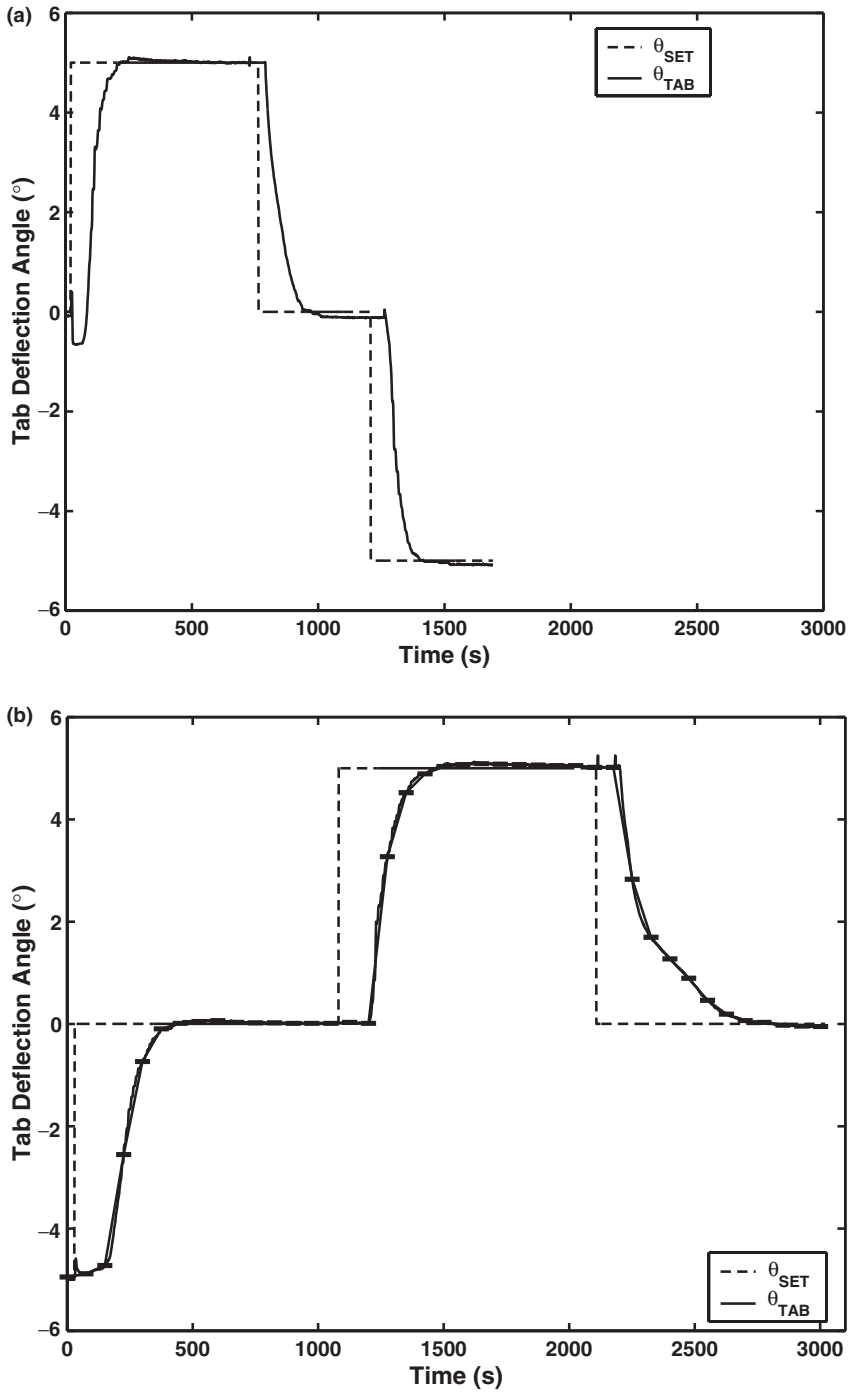

Figure 12. *Time trace of the tracking response for tab up and down inputs of 5° for zero and maximum load conditions: (a) Zero load test; (b) maximum simulated load test.*

demonstrates zero overshoot for all cases, regardless of loading. There however, exists a definite trade-off in overall closed-loop response characteristics of the system. This is evident when evaluating the excellent overshoot characteristics in conjunction with large rise and settling times, which are of the order of 200 s for almost all wind loading conditions. It is possible to reduce these characteristic times but this will result in a degradation in output overshoot behavior. The closed-loop system response may be controlled by tuning the PID control system gains according to the desired closed-loop characteristics.

These results may be compared with test results for the same actuator, integrated with both two position and proportional closed-loop control schemes. The results from these tests are discussed in detail in Singh (2002). For these two control cases the actuator demonstrated large amplitude overshoot and

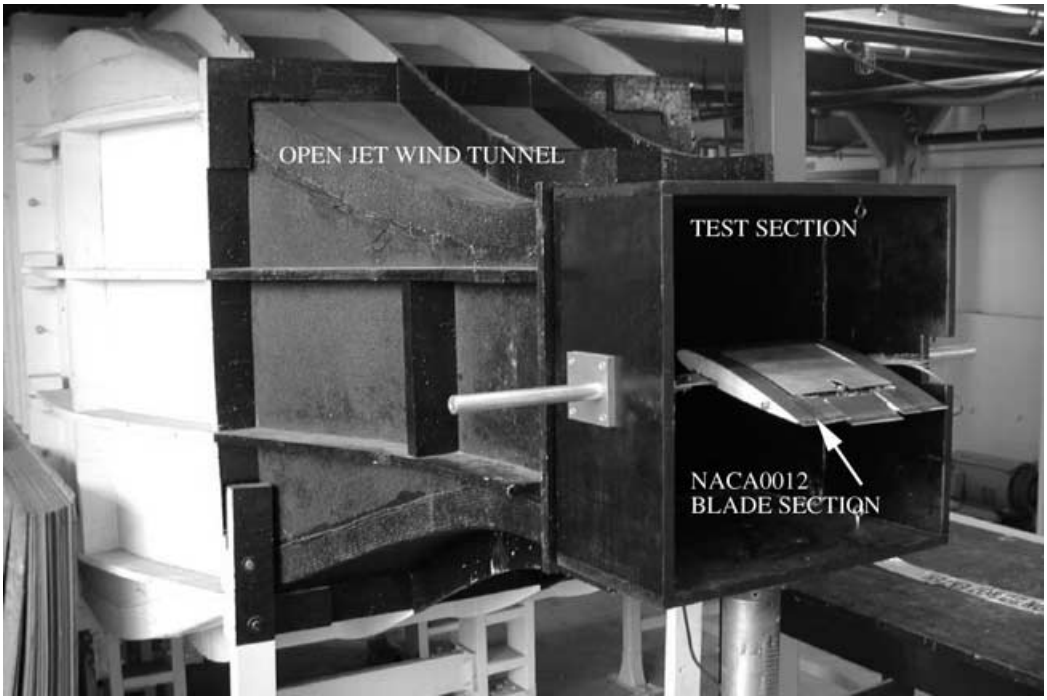

Figure 13. *Setup for open-jet wind tunnel closed-loop testing of tab actuator.*

oscillations about the set point, although the rise and settling times were much lower and of the order of 10–20 s. Furthermore, the steady state resolution under these control conditions was of the order of 0.2°. These comparisons demonstrate enhanced overall performance of the actuator, with PID closed-loop control.

CONCLUSIONS

An SMA tab actuator for rotor blade tracking was designed and tested. The actuator employs a simple mechanism for bidirectional actuation using two sets of antagonistic SMA wires. The advantage of using an SMA actuator is the relatively large output force and deflection angle capability that ensures a simple actuator design with a minimum number of moving parts. The fundamental elements of this system are the SMA wires, a passive friction brake and a PID control system to enable closed loop tracking of the tab. The entire system was embedded into a NACA 0012 blade section with a 12 in. chord.

An analytical model of the actuator was developed to predict the output characteristics under varying external loading conditions. The analysis incorporated thermo-mechanical modeling of the SMA wires using Brinson's model, effect of external loads and the effect of the passive friction brake. The model was validated by open-loop bench top tests performed on the actuation system and good correlation was obtained. Parametric studies were carried out to size the actuator, based on predicted external loading conditions. Based on the assessment of the blade profile, it was determined that the relative flexibility in spanwise dimension and constraint in chordwise dimension allowed for the definition of a primary actuator sizing parameter, the number of wires . This parameter was observed to have a direct influence on the maximum operating wind speed in which the actuator could deflect the tab. This control parameter was iterated to determine the final parameter values for sizing the complete actuator.

Closed-loop tests with a PID controller were performed on the tracking tab at wind speeds of up to 120 ft/s and a maximum angle of attack of 15°. The results demonstrated the actuator was capable of consistent, repeatable tracking with a resolution of less than 0.05°, up to tab deflection angles of 5°, accompanied by the desired position hold under power-off conditions. The gains for the PID controller resulted in good performance at all the tested loading conditions, however, the system did exhibit relatively slow rise and settling times of the order of 200 s. In contrast, the actuator when tested earlier with both simple two position and proportional control systems, demonstrated large amplitude overshoot and oscillations prior to reaching steady state conditions. Under these control laws however, the actuator had lower rise and settling times, of the order of 10–20 s. However, the steady state conditions under PID control are much improved and overall the good resolution, minimal overshoots, and zero oscillations demonstrated marked

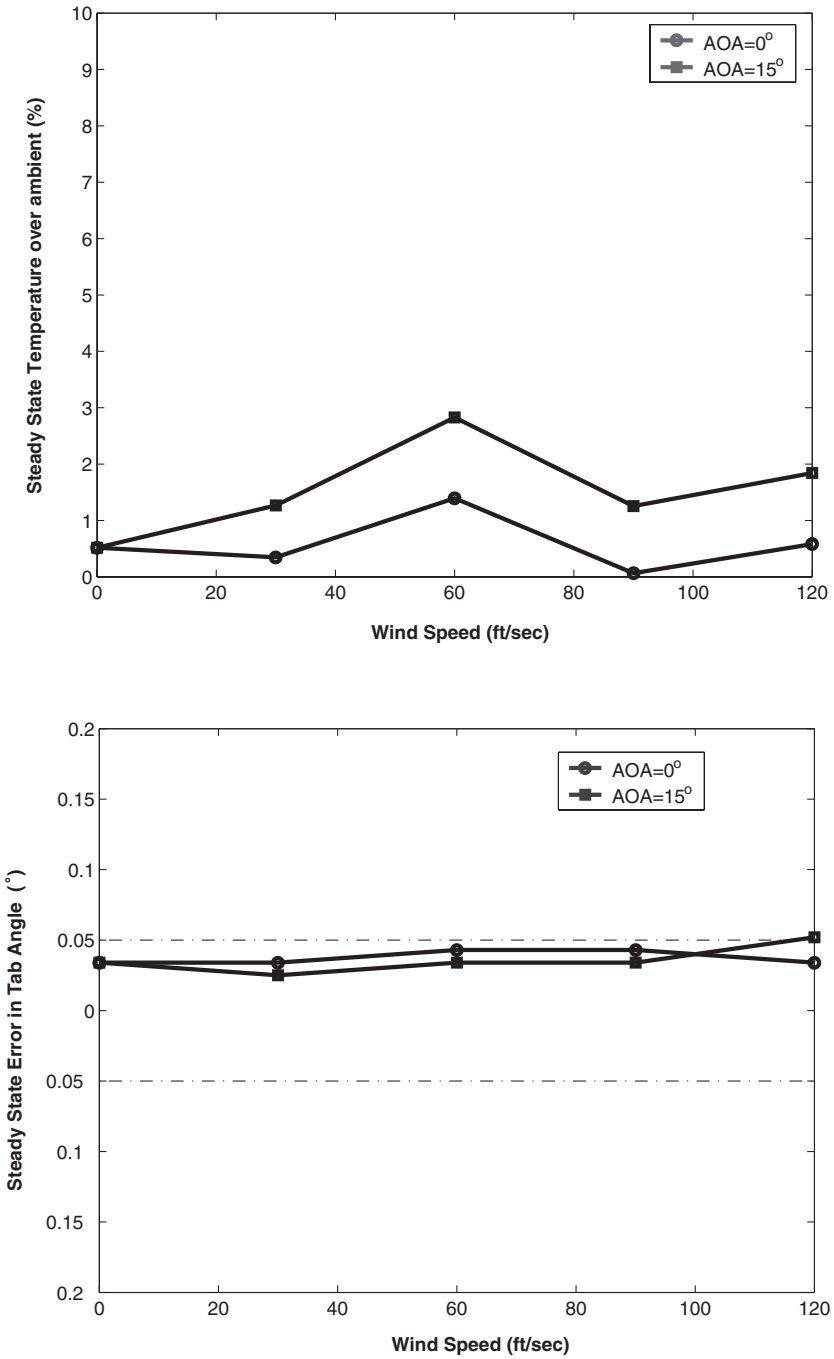

Figure 14. *Influence of wind speed and angle of attack on actuator steady-state conditions for tracking input of 5°: (a) Steady state error; (b) steady state temperature (percentage increment over ambient conditions).*

improvements over the previous design. Test results suggest that although the system is highly nonlinear, it can be accurately controlled using only a simple single input, single output PID controller with constant gains. For improved performance over the entire operating range, the control gains may be changed depending upon the loading condition. Thus a gain scheduling approach would be highly recommended.

The results from this study seem to suggest that the next course of action should involve rotating frame tests. For that purpose, additional structural modifications would be required for testing operational capability at centrifugal loads and at air loads expected at the 75% radial station of the blade. In order to test for full-scale tab actuation, tab sizing issues need to be addressed. In addition, weight saving measures should

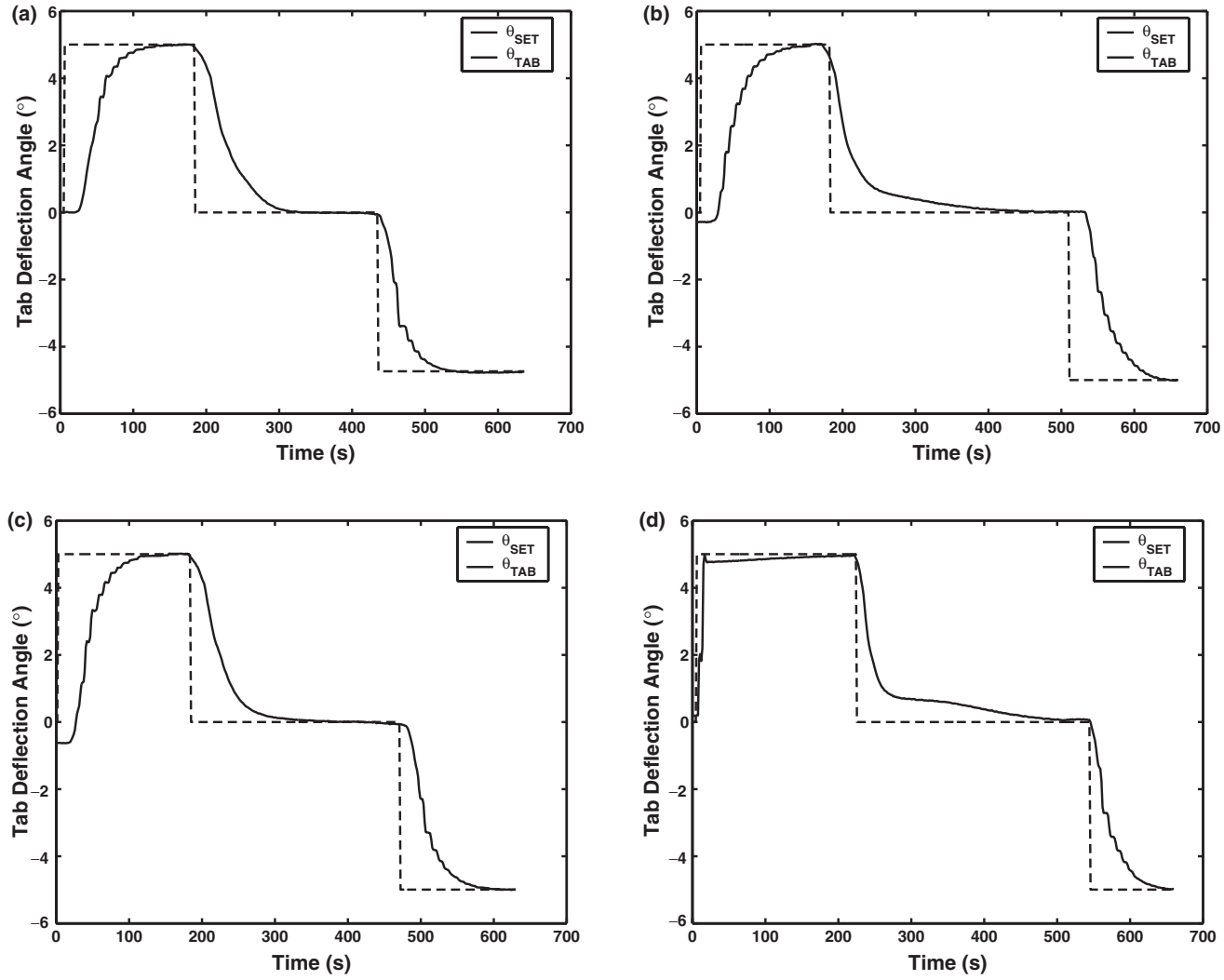

Figure 15. *Time trace of the tracking response for tab up and down inputs of 5° for representative wind conditions: (a) V = 0 ft/s, α = 0°; (b) V = 120 ft/s, α = 0°; (c) V = 30 ft/s, α = 15°; (d) V = 120 ft/s, α = 15°;*

be implemented to ensure that a spanwise increment of actuator dimensions does not result in prohibitively large actuator weight.

NOMENCLATURE

T = temperature (F)
σ = stress (psi)
ϵ_r = recovery strain
ξ = martensite fraction
ξ_T = temperature induced martensite fraction
θ = shaft rotation (°)
L_o = length of SMA wire (in.)
r_{ht} = radius of hinge tube (in.)
l = lift per unit length (lbs/in.)
C_l = lift coefficent
h = hinge moment per unit length (in lbs/in.)
C_h = hinge moment coefficent
c_f = flap chord (in.)
V = wind speed (ft/s)
ρ = air density (slugs/ft^3)
δ = flap (tab) deflection angle (°)
U_{PID} = PID actuation voltage (V)
V_{SET} = command tab angle (V)
K_P = proportional gain
K_I = integral gain

Superscripts

A = parameter corresponds to wire A
B = parameter corresponds to wire B
E = Young's Modulus (psi)
ϵ = strain
ϵ_l = maximum recoverable strain
τ = moment (in. lbs)
ξ_S = stress-induced martensite fraction
Ω = phase transformation coefficient
d_o = diameter of SMA wire (mil)
N_{wire} = number of SMA wires

L = total lift (lbs)
C_{l_α} = lift curve slope ($^{\circ -1}$)
H = total hinge moment (in. lbs)
c = blade section chord length (in.)
l_f = flap span (in.)
M = mach number
α = angle of attack ($^\circ$)
$u(t)$ = actuating signal (V)
V_{err} = error in command and feedback (V)
V_{TAB} = feedback tab angle (V)
K_{D} = derivative gain
Δ_{dead} = deadband ($^\circ$)

Subscripts

F = frictional parameter
o = initial value of parameter

REFERENCES

Abbott, I.H. and von Doenhoff, A.E. 1959. *Theory of Wing Sections*, Dover Publications, Inc., New York, N.Y. 10014.

Brinson, L.C. 1993. "One Dimensional Constitutive Behavior of Shape Memory Alloys: Thermomechanical Derivation with Non-constant Material Functions and Redefined Martensite Internal Variables," *J. Intelligent Material Systems and Structures*, 4:229–242.

Dynalloy 2002. Website: 'http://www.dynalloy.com', Flexinol Technical Characteristics, Dynalloy Inc., 3194-A Airport Loop Drive, Costa Mesa, CA.

Epps, J.J. and Chopra, I. 2000. "Methodology for In-flight Tracking of Rotor Blades Using Shape Memory Alloy Actuators," In: *Proceedings of the 56th American Helicopter Society Forum.*

Giurgiutiu, V., Rogers, C.A. and Zuidervaart, J. 1997. "Incrementally Adjustable Rotor-blade Tracking Tab Using SMA Composites," In: *38th AIAA/ASME/ASCE/AHS/ASC*, *Structures*, *Structural Dynamics and Materials Conference*, Kissimmee, FL.

Kennedy, D.K., Straub, F.K., McD. Schetky, L., Chaudhry, Z. and Roznoy, R. 2000. "Development of a SMA Actuator for In-flight Rotor Blade Tracking," In: Wereley, N.M. (ed.), *Smart Structures and Materials 2000: Smart Structures and Integrated Systems*, Vol. 3895 of Proceedings SPIE.

Liang, C., Davidson, F., Schetky, L.M. and Straub, F.K. 1996. "Applications of Torsional Shape Memory Alloys Actuators for Active Rotor Blade Control – Opportunities and Limitations," In: *Smart Structures and Materials 1996*: *Smart Structures and Integrated Systems*, Proceedings SPIE.

Ogata, Katsuhiko 1997. *Modern Control Engineering*, **3rd edn**, Prentice-Hall, Englewood Cliffs, New Jersey 07632.

Prahlad, H. and Chopra, I. 2001. Comparative Evaluation of Shape Memory Alloy Constitutive Models with Experimental Data," In: *Smart Structures and Materials 2001: Smart Structures and Integrated Systems*, *Proceedings SPIE.*

Rediniotis, O.K., Lagoudas, D.C., Garner, L.J. and Wilson, L.N. 1999. "Development of a Spined Underwater Biomimetic Vehicle with SMA Actuators," In: Wereley, N.M. (ed.), *Smart Structures and Materials 1999: Smart Structures and Integrated Systems*, Vol. 3668 of Proceedings SPIE.

Singh, Kiran 2002. "Design of an Improved Shape Memory Alloy Actuator for Helicopter Blade Tracking," Master's Thesis, University of Maryland, Department of Aerospace Engineering, College Park, MD.

Walz, C. and Chopra, I. 1994. Design and Testing of a Helicopter Rotor Model with Smart Trailing Edge Aps," In: *35th AIAA/ASME/ASCE/AHS/ASC*, *Structures*, *Structural Dynamics and Materials Conference*, Hilton Head, SC.